PCCP

PAPER

View Article Online
View Journal | View Issue

Cite this: *Phys. Chem. Chem. Phys.*, 2025, **27**, 25179

Dynamics of lifting the Au(111) reconstruction in perchloric acid electrolyte

Gary S. Harlow,†*[acd] Weronica Linpé,[a] Sebastian Pfaff,[b] Ziyan Yang,[cd] Leon Jacobse,‡[f] Vedran Vonk,[f] Giuseppe Abbondanza,§[a] Marina Peña-Díaz,¶[cd] S. Barja,[cd] Ann-Christin Dippel,[e] Olof Gutowski,[e] Alfred Larsson,[a] Lisa Rämisch,[b] Johan Zetterberg,[b] Lindsay R. Merte,[g] Andreas Stierle[f] and Edvin Lundgren*[a]

Received 2nd September 2025,
Accepted 22nd October 2025

DOI: 10.1039/d5cp03380b

rsc.li/pccp

The striped $p \times \sqrt{3}$ reconstruction of Au(111) is a textbook example of how electrode surfaces reorganise in response to an applied potential. Using *in situ* high-energy surface X-ray diffraction, we track the surface reconstruction in 0.1 M $HClO_4$ electrolyte while the potential is cycled at both 5 mV s^{-1} and 2 mV s^{-1} between 0.06 V and 0.86 V *versus* RHE. Reciprocal-space maps, collected every ~10 s, show that the unit cell of the well-known herringbone reconstruction increases in length progressively as the potential is swept positively; the diffraction spots coalesce with the spot from the (111) surface and the reconstruction lifts completely above ≈0.7 V. The lifting and reformation dynamics of the surface reconstruction are seen to be relatively slow and continuous, when the potential is swept at 5 mV s^{-1} we observe the reconstruction lifting at more positive potentials than when swept at 2 mV s^{-1}. Conversely the reforming of the reconstruction is also slow and is present at more positive potentials when the sweep rate is slower.

The surfaces of single crystal model electrodes in electrochemistry provide important platforms for testing hypotheses about activity, selectivity, and stability of electrocatalysts. Such surfaces also provide an important bridge between experiments and theory, being our closest analogues to the models calculated with theoretical methods like density-functional theory. The Au(111) surface is a popular model electrode thanks to the ease with which clean well-ordered surfaces can be prepared *via* flame annealing. Yet, the interpretation of results are often complicated by the presence of the "striped" $p \times \sqrt{3}$ reconstruction that forms a herringbone type motif under both UHV and electrochemical conditions.[1–4] The surface prepared thermally *via* UHV or flame-annealing has a ~4.5% uniaxial compression (p = 22) relative to the bulk, but in electrolyte the herringbone pattern is more disordered[5] and may have a different stripe separation (and therefore uniaxial compression) depending on the potential, electrolyte, and surface quality. Most theoretical treatments nevertheless assume an unreconstructed, ideal Au(111) slab, neglecting this intrinsic strain and the registry of FCC/HCP stripes.

Perchloric acid ($HClO_4$) is frequently chosen as a "non-specific" supporting electrolyte, as the perchlorate anion (ClO_4^-) is only weakly adsorbing and the cyclic voltammogram (CV) lacks the pronounced lifting or adsorption peaks observed for strongly adsorbing anions such as chloride or sulfate.[6] A direct comparison of the CVs obtained in a baseline 0.1 M $HClO_4$ electrolyte and in one containing an additional 5 mM Cl^- illustrates these differences clearly (Fig. 1). In the Cl^--containing electrolyte, a sharp anodic peak appears around 0.45 V, coinciding with the lifting of the $p \times \sqrt{3}$ reconstruction, while symmetrical peaks near 1.0 V correspond to the disorder–order transition in the adsorbed anion layer. Other specifically adsorbing anions, such as SO_4^{2-} and Br^-, produce similar features, with potential shifts reflecting their adsorption strength and concentration. By contrast, in ClO_4^- electrolytes

[a] *Division of Synchrotron Radiation Research, Lund University, Sweden. E-mail: edvin.lundgren@fysik.lu.se, gharlow@uoregon.edu*
[b] *Division of Combustion Physics, Lund University, SE-22100 Lund, Sweden*
[c] *Department of Chemistry and Biochemistry, University of Oregon, USA*
[d] *Department of Polymers and Advanced Materials, Centro de Física de Materiales, University of the Basque Country UPV/EHU, 20018, San Sebastián, Spain*
[e] *Deutsches Elektronen-Synchrotron (DESY), D-22603 Hamburg, Germany*
[f] *Centre for X-ray and Nano Science CXNS, Deutsches Elektronen-Synchrotron DESY, 22607 Hamburg, Germany*
[g] *Department of Materials Science and Applied Mathematics, Malmö University, Malmö, Sweden*
† Current address: Department of Chemistry and Biochemistry, University of Oregon, USA.
‡ Current address: Department of Interface Science, Fritz Haber Institute of the Max Planck Society, Berlin, Germany.
§ Current address: Department of Physics, Chalmers University of Technology, Chalmersplatsen 4, 41296 Gothenburg, Sweden.
¶ Current address: TECNALIA, Basque Research and Technology Alliance (BRTA), Mikeletegi Pasealekua 2, 20009 Donostia-San Sebastián, Spain.

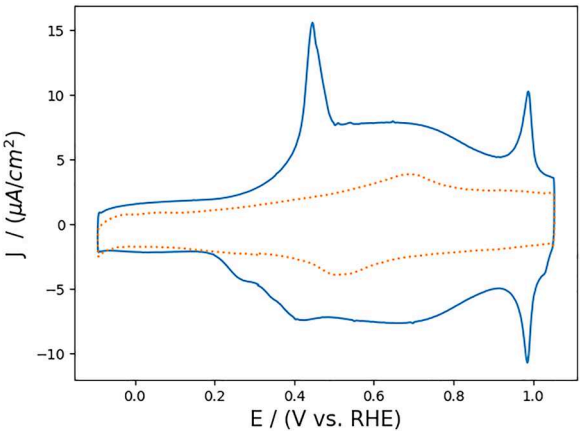

Fig. 1 Cyclic voltammogram of Au(111) electrode in 0.1 M $HClO_4$ electrolyte (broken line), and 0.1 M $HClO_4$ + 5 mM KCl. Sweep rate = 50 mV s^{-1}. The CV was measured *ex situ* with a different Au(111) crystal (but with the same specifications) than the rest of the manuscript. Manual *iR* compensation was applied using 85% of the measured series resistance (0 mM KCl = 85 Ω; 5 mM = 106.5 Ω).

only a broad wave is observed near 0.7 V, with no distinct lifting peak.

This has sometimes led to the incorrect assumption that the Au(111) reconstruction remains largely intact, or at most passively perturbed, during polarization in perchloric acid. However, the extent to which the reconstruction actually responds to interfacial charging in nominally "non-specific" electrolytes remains under reported minus a few notable studies.[5–7] At positive potentials, even in acidic environments, OH adsorption can occur and is known to affect the structure and reactivity of noble metal surfaces, including Au(111) in alkaline.[8–10] Such OH adsorption, combined with changes in interfacial charge density, may drive or modulate reconstruction lifting even in the absence of strongly adsorbing anions, although even on Pt electrodes differentiating between OH mediated $ClO4^-$ adsorption and direct $ClO4^-$ adsorption remains a matter of much debate.[11–13] The resulting lifting process may therefore be more gradual, incomplete, or dynamic than the sharp transition observed for Cl^-.

This ambiguity is not merely academic: reconstruction alters surface stress, step density, and electronic structure, thereby influencing adsorption energetics and interfacial reactivity. As a result, the reconstruction state of Au(111) under electrochemical conditions may not be well defined, complicating the interpretation of measurements and limiting its reliability as a model surface. The present work directly probes this issue by using operando surface X-ray diffraction to monitor reconstruction lifting dynamics in perchloric acid, providing structural insight into a regime where electrochemical signatures alone are inconclusive.

Here we use time-resolved high-energy surface X-ray diffraction (HESXRD) to quantify, in situ, both the average unit-cell parameter p and the associated uniaxial compression of Au(111) in 0.1 M $HClO_4$. Previously surface X-ray diffraction (SXRD) has been used numerous times to probe the static surface reconstruction in a variety of electrolytes[1,9,10,14,15] and we have previously reported high-energy SXRD[16] measurements of Au(111) in 0.1 M H_2SO_4 after going to very oxidizing conditions.[17] These results highlight the advantages of time resolved measurements, and even faster measurements have been demonstrated using a rotating disk-electrode setup.[18] Here we collect complete reciprocal-space maps in less than 3 minutes, capturing the integer (CTR) and reconstruction rods simultaneously. Shorter, rapid, repetitive sweeps let us follow the lifting process as we cycle the potential, we observe the lifting as continuous process where the striped phase expands and finally lifts during a CV scan.

Our results confirm the presence of the surface reconstruction in $HClO_4$ electrolyte up to much more positive potentials than for halides like Cl^- and Br^-, or other more strongly adsorbing anions like SO_4^{2-}. We also reveal (i) the lifting process is kinetically sluggish, occurring at more positive potentials when the sweep rate is raised from 2 to 5 mV s^{-1}, (ii) both the lifting and formation of the reconstruction are gradual processes where defects across a larger unit cell converge to form the stripped phase, (iii) all long-range ordering in the reconstruction has vanished by ~0.7 V *vs.* RHE, (iv) stripe separation, p, may have values that deviate significantly from the ideal UHV value of p = 22.

Experiment

The electrochemical cell was a flow cell constructed from PEEK™ which we have previously reported,[19] Fig. 2 shows an illustration of the cell on the diffractometer. The glassware, ETFE HPLC fittings, Kalrez™ O-rings were cleaned in piranha solution consisting of 3 : 1 98% H_2SO_4 and 30% H_2O_2 for 2 hours. The cell was left in 65% HNO_3 acid for 8 hours. All parts were then rinsed twice in ultrapure water (18.2 MΩ cm) and boiled five times with two further rinses in between. The perfluoroalkoxy (PFA) tubing was cleaned by running a 10% dilute piranha solution through with the peristaltic pump for

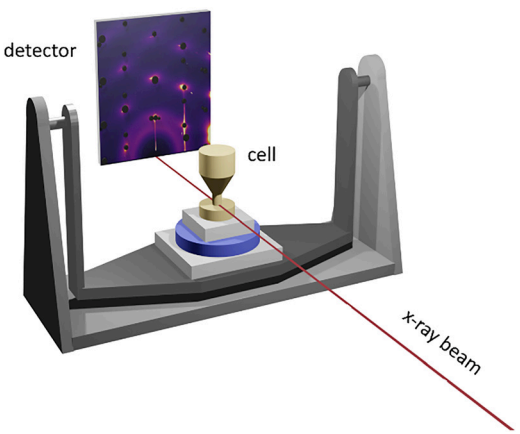

Fig. 2 Schematic of experimental setup, an electrochemical cell is rotated in grazing incidence geometry and the diffraction is collected *via* a large area detector. Tungsten beam stops blackout Bragg spots.

several hours. There was a short section of peristaltic pump tubing which was Masterflex™ Chem-Durance Bio. Several litres of ultrapure water were also pumped through the cell. The gold counter-electrode was submerged in 65% nitric acid at 60 °C, rinsed several times in ultrapure water and then flame annealed before assembly. The reference electrode was a 'leak-less' Ag/AgCl reference electrode purchased from eDAQ, prior to the experiment it was tested by performing a cyclic-voltammogram in 0.1 M H_2SO_4, after which it was then rinsed multiple times in ultrapure water then in 20% nitric acid followed by more rinses in ultrapure water. All potentials quoted in the paper are converted to the reversible hydrogen electrode (RHE) to allow easier comparison with literature, where $E_{Ag/AgCl(3.4\ M)}$ = +0.205 V *vs.* SHE. The pH of 0.1 M $HClO_4$ was measured to be 1.02 ± 0.02 at 25 °C (3 measurements) with a freshly calibrated Orion Lab Star PH111 Bench pH Meter, given the small deviation (1.2 mV) compared to other sources of error a value of 1.0 was used. Therefore, $E_{RHE} = E_{meas}$ + 0.205 V +0.059 V at 25 °C. The Au(111) single crystal had a diameter of 6 mm and was purchased from Mateck GmbH, Germany, the purity is 99.999% with a surface roughness <0.01 μm and aligned to $<0.1^\circ$. Before use it was placed in 65% nitric acid at 60 °C for 5 minutes and rinsed, it was then oxidised in 0.1 M sulphuric acid for 20 s at 10 V, rinsed and then stripped in 1 M HCl, and again rinsed multiple times. Prior to the experiment, it was flame annealed in a butane flame, and after transfer to the electrochemical cell the potential was cycled 20 times in the electrolyte solution (0.1 M $HClO_4$) over the range 0.064 to +0.864 V *vs.* RHE at 50 mV s^{-1} and then held at 0.264 V. This was to ensure reproducible surface preparation ('surface conditioning') in each case, as we have previously observed the long-range order of the electrochemical reconstruction increasing with initial cycles, this also means that we never measure the thermally induced surface reconstruction, and only the electrochemically induced reconstruction.

The HESXRD measurements were performed on beamline P07, second experimental hutch EH2, at Petra III, DESY using a focused incident X-ray of energy 73 keV (λ = 0.168 Å), the vertical beam height was around 2 μm, and the sample was aligned to have an incidence angle of 0.07°. The sample-detector-distance was 1.6 m. We used a PerkinElmer flat panel X-ray detector especially suited for high X-ray photon energies. The detector consists of an array of 2048 by 2048 pixels, each 200 × 200 μm^2. The Bragg reflections were blocked by placing tungsten beam stops on a plastic screen in front of the detector. Fig. 2 illustrates the HESXRD experimental geometry used. The hexagonal unit cell we use is defined such that the surface

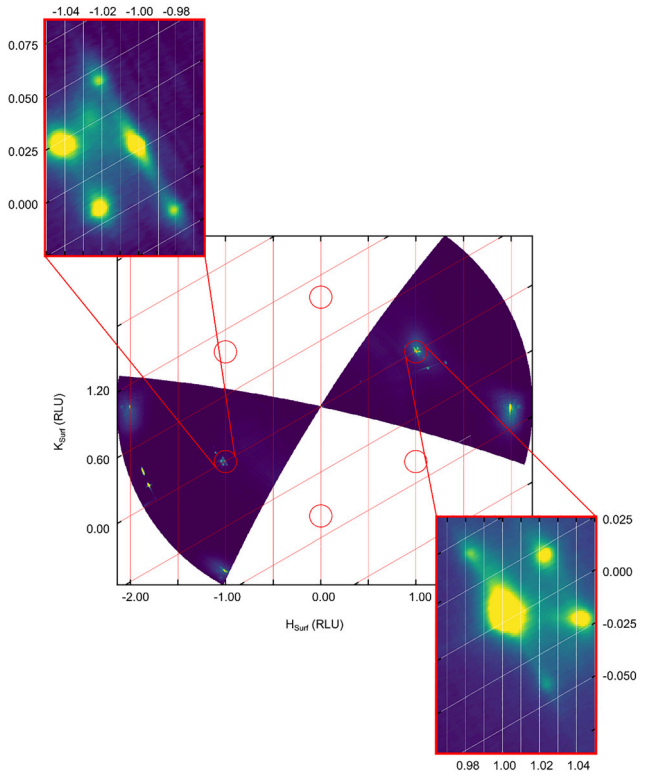

Fig. 3 Reciprocal space map in the HK plane for a 70° sample rotation. Reciprocal space values in the range $0.15 < L < 0.25$ were binned on a 1600 × 1600 gird. A Gaussian filter has been applied to these images, but not later reciprocal space maps. The electrode position was held at 0.064 V *vs.* RHE.

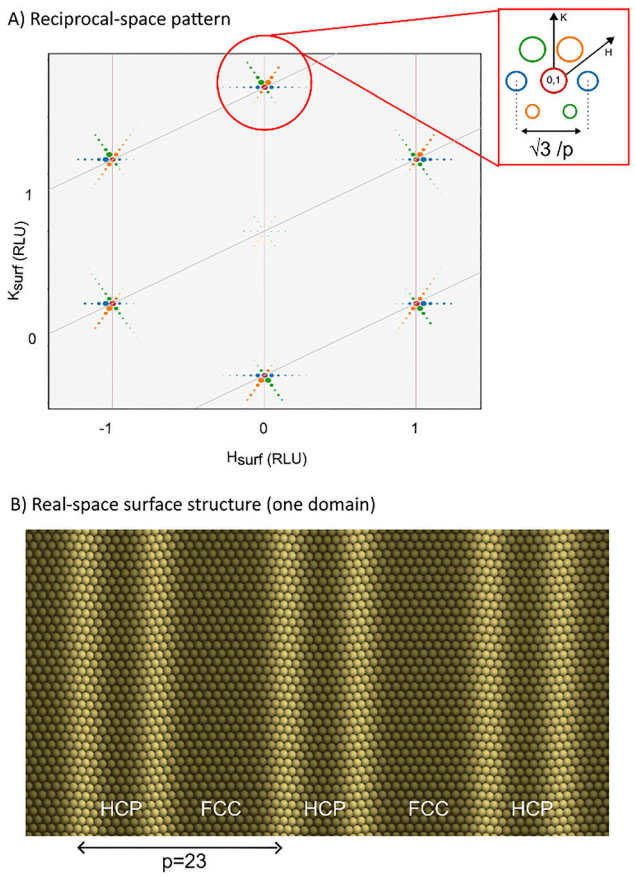

Fig. 4 (A) Calculated reciprocal space map for the Au(111) surface reconstruction in hexagonal surface units. Stripe separation, *p*, can be directly calculated from the position of the diffraction spots. (B) Real-space structure used to generate diffraction pattern.

normal is along the $(0, 0, L)_{hex}$ direction and the $(H, 0, 0)_{hex}$ and $(0, K, 0)_{hex}$ vectors lie in the plane of the surface and subtend 60°. The units for H, K and L are $a^* = b^* = 4\pi/\sqrt{3}a_{NN}$ and $c^* = 2\pi/\sqrt{6}a$, where a is the nearest-neighbour distance in the crystal (a = 2.884 Å). Due to ABC stacking along the surface normal direction, the unit cell contains three atomic layers and the Bragg reflections (blocked by beam-stops) are spaced apart by multiples of three in L.

Results and discussion

During data collection the aligned sample was rotated about its surface normal. By selecting the maximum intensity of each pixel across the rotation (maxed image) or summing the images, one gets an immediate and accessible view of reciprocal space. We have developed a software package, based on several previously described calculations, called the HESXRD-Analysis-Toolkit (HAT),[20] which converts the pixel positions for each image in a rotation to reciprocal space positions and generates a reciprocal space map, either in units of momentum transfer (Q) or reciprocal lattice units (RLU). Initially the potential was held at 0.064 V, a potential at which the surface is known to be reconstructed. A dataset consisting of 1400 images was collected (over a 70° rotation, see SI, Movie S1), meaning each 2048 × 2048 pixel image is the integration of 0.05° of sample rotation. This is shown as a reciprocal space map in Fig. 3 created by plotting the summed intensity ($0.15 < L < 0.25$) on the H and K axes. There are two CTRs rods at HK = (−1, 0) and (1,0). Due to the ABC stacking of the bulk crystal and it's 3-fold symmetry around the (111) the diffraction pattern has 120° symmetry and therefore they are not symmetry equivalent reflections. At $HK \sim -1.03$ and +1.03 there are additional rods of scattering, which are superpositions of the non-integer scattering rods due the $p \times \sqrt{3}$ surface reconstruction. A video showing the detector view and in-plane reciprocal space map collected as l = 0.2 as the sample is rotated is available in SI. Our measured reciprocal space map can be compared to a simulated one (Fig. 4A) calculated p = 23 and observations of the stripe width from UHV STM measurements, a general agreement can be seen. A real-space model for one domain of this is shown in Fig. 4B.

At higher potentials it is known that the surface reconstruction lifts due to either charge or anion adsorption (this remains a point of debate), after the $p \times \sqrt{3}$ surface reconstruction has lifted, only the CTR on the integer RLU coordinates is observed.

The total collection time for the data presented in Fig. 3 was around 140 s. While such a time is quick compared to conventional reciprocal space mapping, it is far slower than a typical cyclic voltammogram. One solution to this is to make short

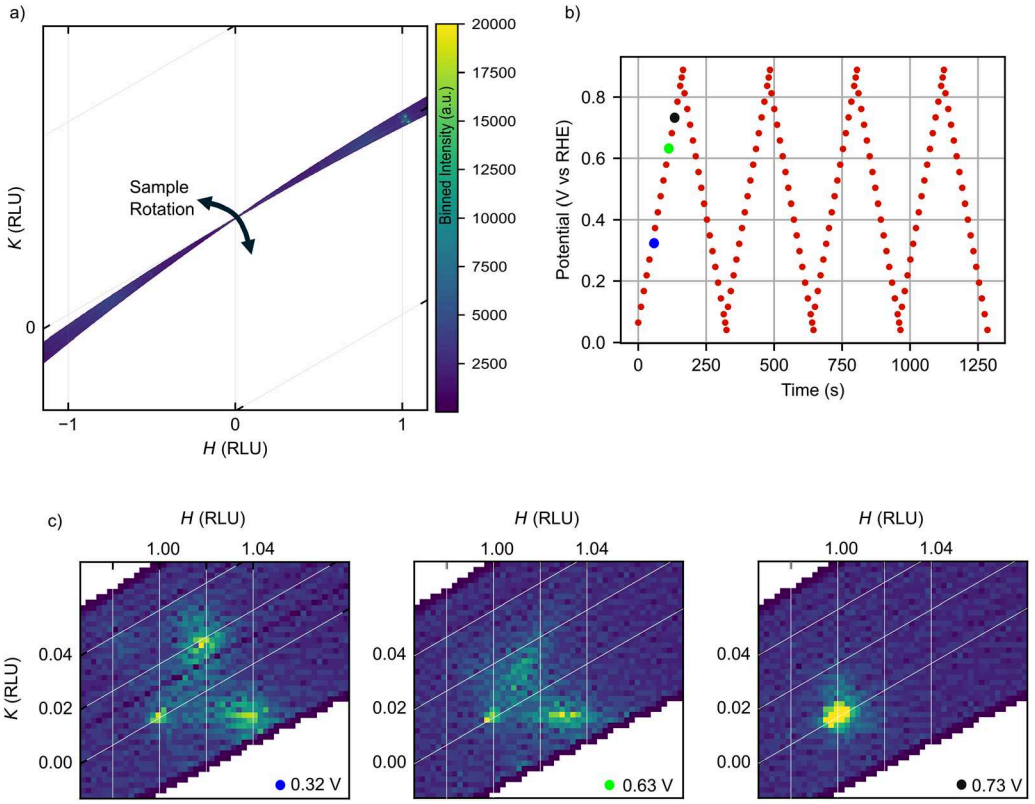

Fig. 5 (a) Shows the region of reciprocal space measured during a short sample rotation taking ~10 s. (b) Each point corresponds to the time when a rotation completed and the potential the applied potential at the start of the next rotation, simultaneously the potential was linearly sweep between 0.064 V and 0.864 V (*vs.* RHE) at a rate of 5 mV s^{-1}. (c) Reciprocal space maps in the HK plane near the (1,0) CTR around $0.15 < L < 0.25$ at different potentials (indicated in b). Color scale is the same as (a).

repetitive scans in both directions, to capture the evolution of a particular region of reciprocal space on a shorter time scale. In this way CTRs and other rods can be captured simultaneously at more relevant time scales. For this experiment we did 4° rotations in both directions, which gave one complete measurement every ∼10 s, including the acceleration and deceleration of the rotation motor. The region of reciprocal space (projected on to the *HK* plane), that is 'swept-out' by such as scan is shown in Fig. 5a where the arrows indicate the sample is rotated in both directions, this region intercepts the (1,0) CTR. Fig. 5b shows the electrode potential as a function of time, where each point indicates when a measurement completed. Fig. 5c shows the region of reciprocal space at several potentials before and during the lifting process. During the positive going anodic potential sweep the diffraction spots from the surface reconstruction begin to move towards the CTR around 0.6 V, suggesting an enlargement of the surface unit just before lifting. At around 0.7 V only the CTR diffraction spot remains suggesting the reconstruction is fully lifted.

We can obtain further information on the surface reconstruction by taking a cut through the CTR and reconstruction rod and then fitting a profile. Fig. 6a shows the detector image collected during one of the quick sweeps described above. The axes are in reciprocal lattice units (RLU) with magnitude of the in-place vector ($HK = Q_r$) along the *x*-axis. The maximum intensity for each pixel across the short rotation is display. In Fig. 6b a magnified region of the detector image is present, the red square indicates the region of interest (ROI) which we integrate, around $L = 0.2$. To avoid integrating multiple symmetry equivalent reconstruction peaks we only use a subset of the rotation shown in Fig. 6c where only the peak with $k > 0$ is integrated. This ROI is summed along the *L*-axis to obtain a line profile that has two peaks such as in Fig. 6d one due to the CTR at $H = 1$, $K = 0$ and one from the surface reconstruction. Fig. 6d shows three profiles one before the lifting (0.4 V), one just before the complete lifting and one after the reconstruction has lifted. In Fig. 7 the line profiles from the entire dataset are plotted as a function of time, during the cyclic voltammetry measurement, Fig. 7a shows 4 cycles at 5 mV s^{-1} and Fig. 7b shows two cycles at 2 mV s^{-1}. It can be observed that the first line profiles show a more intense reconstruction peak in Fig. 7a, this must because previously the potential was only ever briefly at the

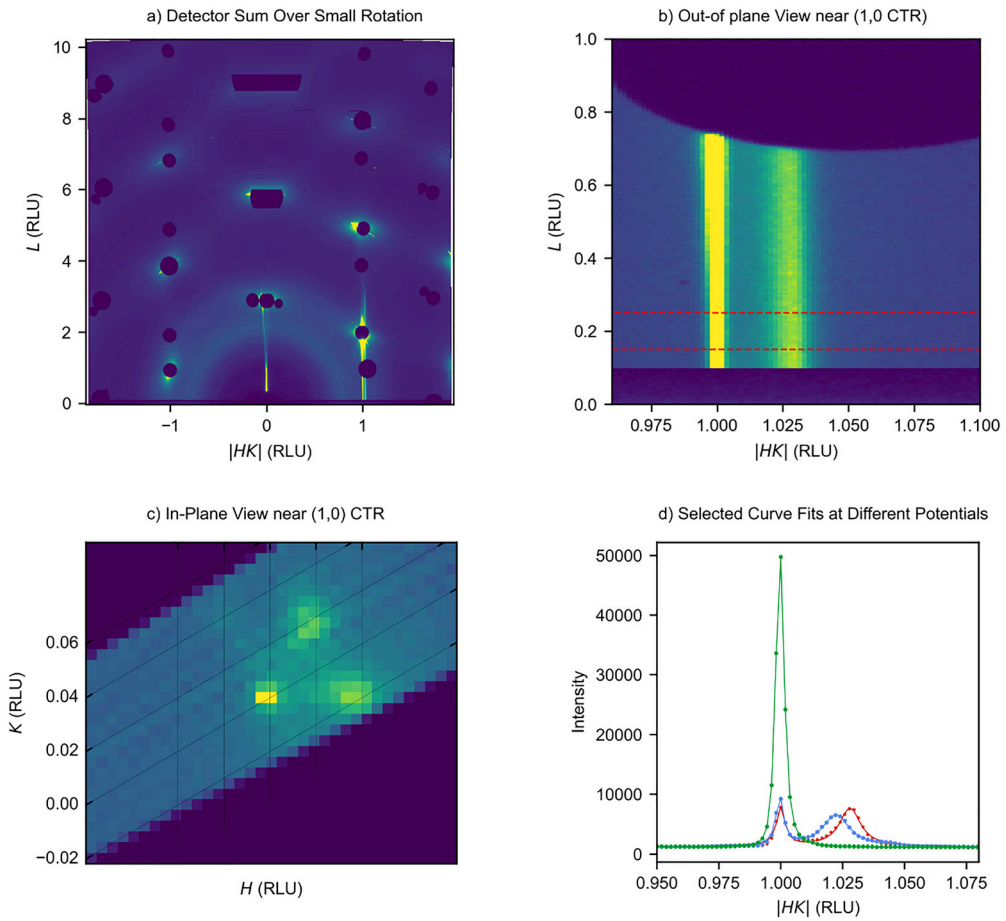

Fig. 6 (a) Detector image transformed to reciprocal space over short sample rotation. (b) Magnified region of the detector image showing the region that is later extracted. (c) In-plane view of reciprocal space analysed, only one reconstruction peak in included in integration. (d) Several line profiles and fits during the cyclic voltammogram. Red is at ∼0.32 V, blue is just before the reconstruction lifts (∼0.63 V) and green at 0.73 V. Points represent measured intensity and solid lines the best fit.

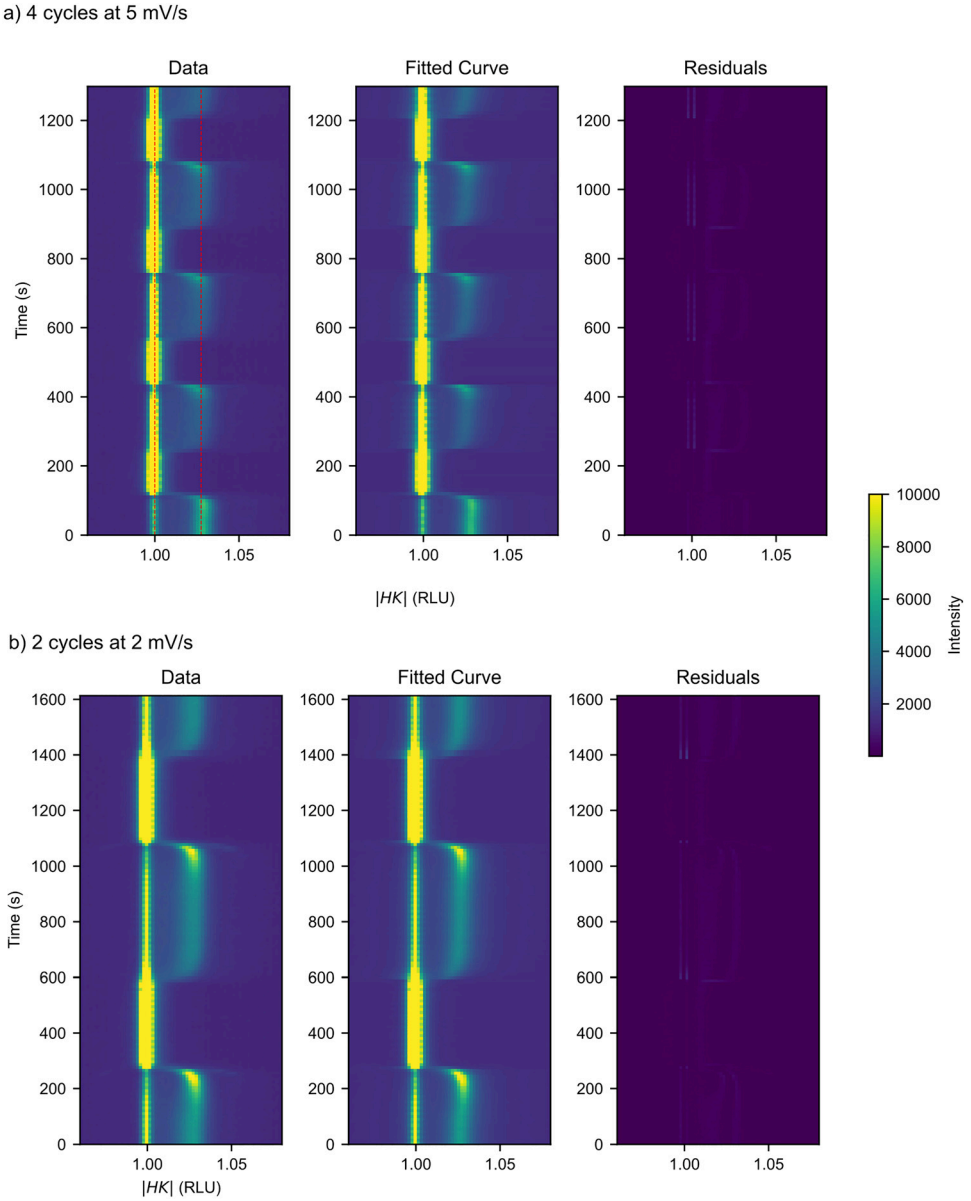

Fig. 7 Evolution of the line profile as a function of potential. Data shows the line-profile extracted as in Fig. 6 as a function of time, Fitted Curve shows the temporal evolution of the fits to that data, and Residuals is the difference between the data and the fits. (a) Cycles at 5 mV s^{-1}, (b) cycles at 2 mV s^{-1}.

positive limit (while cycling t 50 mV s^{-1}) – after the slower scan at 5 mV s^{-1} the intensity of the reconstruction never fully recovers. The position of the reconstruction peaks can be seen to move towards the CTR position as the potential is increased and move outwards when the reconstruction is reformed on the reverse sweep. Each line profile like those in Fig. 6d can be individually fit with a two Lorentzian profiles and a linear background, as previously described,[14] this is valid and based on a 1D real space atomic model in which the correlation length (f) decays exponentially with a length $f = a/(2\pi\sigma)$, where σ is the full width half maximum (FWHM). The difference in position of the peak centres from the CTR peak can be used to calculate the stripe separation, which is a distance in multiples of the lattice constant a. The best fits that were obtained *via* non-linear least-squares fitting are shown in Fig. 7 and the residual of the fits (also shown) indicates a reasonable level of agreement across the dataset (<2.9%).

The stripe separation (p) determines the position of the reconstruction peak in the data shown in Fig. 7, which we can extract as a function of potential or time.

Fig. 8a shows a plot of how the stripe separation (in units of the lattice constant) varies with potential while cycling at 5 mV s^{-1} and 2 mV s^{-1} and Fig. 8b shows how the correlation length of the reconstruction also changes. In the forward anodic sweeps, as the potential is increased, the stripe separation decreases and the correlation length increases, this indicates that just before the reconstruction lifts it has the highest long-range order and a stripe separation closer to that found in UHV. Notably the stripe separation is always considerable higher than the UHV

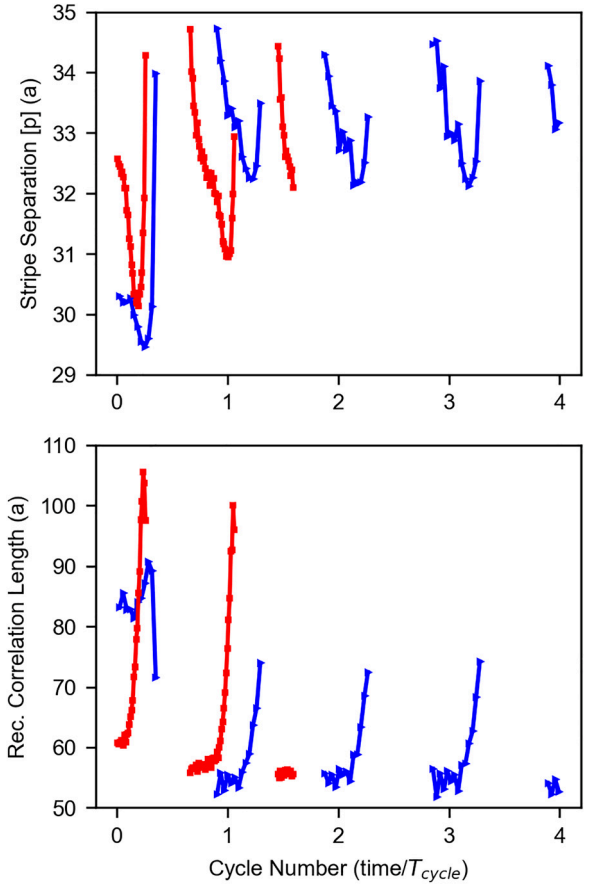

Fig. 8 Variation of calculated parameters from fits to reconstruction scattering (a) stripe separation and (b) correlation length with applied potential at two scan rates – 2 mV s^{-1} and 5 mV s^{-1}, the gaps are where no surface reconstruction was detected.

value of p = 22. The x-axis in Fig. 8 has been normalized by the measurement time so that the different potential sweep rates can be compared. In Fig. 8 the reconstruction can be seen to lift earlier (at a more negative potential) and reforms sooner on the reverse sweep (at a more positive potential) for the 2 mV s^{-1} sweep rate (squares) than when the potential was swept at 5 mV s^{-1} (triangles). This is because the lifting and forming of the reconstruction is a slow process that involves the movement of surface atoms, therefore gold surfaces may look very different at different sweep rates and this should be considered when designing experiments. It is also clear that formation and lifting of the Au(111) surface reconstruction is not a sudden phase change but rather a continuous change in the registry of the top layer of the gold surface. Furthermore, the presence of the surface reconstruction in perchloric acid is confirmed and the potential that the reconstruction lifts is more positive than for electrolytes containing halides or sulphates, it occurs at a potential where a small peak is seen in the CV.

Conclusions

By leveraging High-Energy Surface X-ray Diffraction (HESXRD), we successfully probe the electrochemical interface of the Au(111) electrode in 0.1 M HClO4 electrolyte, measuring the surface scattering from its characteristic $p \times \sqrt{3}$ surface reconstruction. We demonstrate the effectiveness of our *in situ* approach by generating time-resolved reciprocal space maps, which enables a direct and detailed observation of the dynamics of this surface reconstruction under potentiodynamic conditions. Processes such as the formation and lifting of surface reconstructions can be relatively slow, meaning that any structure captured at a static potential may not represent true surface structure during potential cycling.

We find that Au(111) is reconstructed in 0.1 M $HClO_4$ electrolyte but has a larger stripe separation than typically found in UHV (p = 31 *vs.* p = 22) and the reconstruction can be reversibly lifted and reformed by controlling the applied potential. The lifting of the Au(111) surface reconstruction is a slow process, with its lifting at more positive potentials when the sweep rate is increased to 5 mV s^{-1} as compared to 2 mV s^{-1}. The lifting and formation of the reconstruction are also seen to be gradual processes where defects across a larger unit cell converge to form the stripped phase. The coherent surface reconstruction detectable by surface diffraction is fully lifted around 0.7 V *vs.* RHE in this electrolyte.

Conflicts of interest

The authors declare that they have no known competing financial interests or personal relationships that could have appeared to influence the work reported in this paper.

Data availability

The data that support the findings of this study are openly available by contacting the corresponding authors. The authors confirm that the data supporting the findings of this study are available within the article and its supplementary information (SI). Supplementary information: movie S1: A ~70° rotation of the Au(111) during surface diffraction in a 0.1 M $HClO_4$ electrolyte at a potential of 0.064 V_{RHE}. See DOI: **https://doi.org/10.1039/d5cp03380b**.

Acknowledgements

We acknowledge DESY (Hamburg, Germany), a member of the Helmholtz Association HGF, for the provision of experimental facilities. This research was carried out at P07 PETRA III. This work was financially supported by the Swedish Research Council through the Röntgen-Ångström Cluster "*In situ* High Energy X-ray Diffraction from Electrochemical Interfaces (HEXCHEM)" (Project no. 2015-06092). S. B. thanks support from the projects Basque Government (IT-1591-22).

References

1 J. Wang, A. J. Davenport, H. S. Isaacs and B. M. Ocko, Surface Charge—Induced Ordering of the Au(111) Surface,

Science, 1992, **255**(5050), 1416–1418, DOI: **10.1126/science.255.5050.1416**.

2 K. P. Bohnen and D. M. Kolb, Charge- *versus* Adsorbate-Induced Lifting of the Au(100)-(Hex) Reconstruction in an Electrochemical Environment, *Surf. Sci.*, 1998, **407**(1–3), L629–L632, DOI: **10.1016/S0039-6028(98)00232-5**.

3 B. M. Ocko, J. Wang, A. Davenport and H. Isaacs, In Situ X-Ray Reflectivity and Diffraction Studies of the Au(001) Reconstruction in an Electrochemical Cell, *Phys. Rev. Lett.*, 1990, **65**(12), 1466–1469, DOI: **10.1103/PhysRevLett.65.1466**.

4 P. A. Thiel and P. J. Estrup, *The Handbook of Surface Imaging and Visualization*, CRC Press, Boca Raton, 1995.

5 C. Vaz-Domínguez, A. Aranzábal and A. Cuesta, In Situ STM Observation of Stable Dislocation Networks during the Initial Stages of the Lifting of the Reconstruction on Au(111) Electrodes, *J. Phys. Chem. Lett.*, 2010, **1**(14), 2059–2062, DOI: **10.1021/jz1006803**.

6 F. J. Rodríguez Nieto, G. Andreasen, M. E. Martins, F. Castez, R. C. Salvarezza and A. J. Arvia, Scanning Tunneling Microscopy, Voltammetry, and X-Ray Photoelectron Spectroscopy Study of the Early Stages of Electrochemical Faceting of Gold (111) in Aqueous Sulfuric and Perchloric Acid, *J. Phys. Chem. B*, 2003, **107**(41), 11452–11466, DOI: **10.1021/jp0353542**.

7 A. Adnan, S. Behjati, N. Félez-Guerrero, K. Ojha and M. T. M. Koper, Tracking the Surface Structure and the Influence of Cations and Anions on the Double-Layer Region of a Au(111) Electrode, *Phys. Chem. Chem. Phys.*, 2024, **26**(32), 21419–21428, DOI: **10.1039/D4CP02133A**.

8 M. Nakamura, Y. Nakajima, K. Kato, O. Sakata and N. Hoshi, Surface Oxidation of Au(111) Electrode in Alkaline Media Studied by Using X-Ray Diffraction and Infrared Spectroscopy: Effect of Alkali Metal Cation on the Alcohol Oxidation Reactions, *J. Phys. Chem. C*, 2015, **119**(41), 23586–23591, DOI: **10.1021/acs.jpcc.5b07878**.

9 Y. Gründer, G. S. Harlow, E. Cocklin, J. Fogg, J. W. Beane and C. A. Lucas, Potential-Dependent Surface Compression of Gold and Its Link to Electrocatalytic Reactivity, *Surf. Sci.*, 2019, **680**, 113–118, DOI: **10.1016/j.susc.2018.10.020**.

10 M. E. Gallagher, B. B. Blizanac, C. A. Lucas, P. N. Ross and N. M. Marković, Structure Sensitivity of CO Oxidation on Gold Single Crystal Surfaces in Alkaline Solution: Surface X-Ray Scattering and Rotating Disk Measurements, *Surf. Sci.*, 2005, **582**(1–3), 215–226, DOI: **10.1016/j.susc.2005.03.018**.

11 G. A. Attard, A. Brew, K. Hunter, J. Sharman and E. Wright, Specific Adsorption of Perchlorate Anions on Pt{hkl} Single Crystal Electrodes, *Phys. Chem. Chem. Phys.*, 2014, **16**(27), 13689–13698, DOI: **10.1039/C4CP00564C**.

12 J. Huang, Zooming into the Inner Helmholtz Plane of Pt(111)–Aqueous Solution Interfaces: Chemisorbed Water and Partially Charged Ions, *JACS Au*, 2023, **3**(2), 550–564, DOI: **10.1021/jacsau.2c00650**.

13 N. Fröhlich, J. Fernández-Vidal, F. V. Mascaró, A. J. Shih, M. Luo and M. T. M. Koper, Effect of Trace Impurities in Perchloric Acid on Blank Voltammetry of Pt(111), *Electrochimica Acta*, 2023, **466**, 143035, DOI: **10.1016/j.electacta.2023.143035**.

14 J. Wang, B. M. Ocko, A. J. Davenport and H. S. Isaacs, X-Ray-Diffraction and -Reflectivity Studies of the Au(111)/Electrolyte Interface: Reconstruction and Anion Adsorption, *Phys. Rev. B: Condens. Matter Mater. Phys.*, 1992, **46**(16), 10321–10338, DOI: **10.1103/PhysRevB.46.10321**.

15 F. Reikowski, T. Wiegmann, J. Stettner, J. Drnec, V. Honkimäki, F. Maroun, P. Allongue and O. M. Magnussen, Transmission Surface Diffraction for Operando Studies of Heterogeneous Interfaces, *J. Phys. Chem. Lett.*, 2017, **8**(5), 1067–1071, DOI: **10.1021/acs.jpclett.7b00332**.

16 J. Gustafson, M. Shipilin, C. Zhang, A. Stierle, U. Hejral, U. Ruett, O. Gutowski, P.-A. Carlsson, M. Skoglundh and E. Lundgren, High-Energy Surface X-Ray Diffraction for Fast Surface Structure Determination, *Science*, 2014, **343**(6172), 758–761, DOI: **10.1126/science.1246834**.

17 W. Linpé, L. Rämisch, G. Abbondanza, A. Larsson, S. Pfaff, L. Jacobse, J. Zetterberg, L. Merte, A. Stierle, Z. Hegedues, U. Lienert, E. Lundgren and G. S. Harlow, Revisiting Optical Reflectance from Au(111) Electrode Surfaces with Combined High-Energy Surface X-Ray Diffraction, *J. Electrochem. Soc.*, 2021, **168**(9), 096511, DOI: **10.1149/1945-7111/ac2702**.

18 L. Jacobse, R. Schuster, J. Pfrommer, X. Deng, S. Dolling, T. Weber, O. Gutowski, A.-C. Dippel, O. Brummel, Y. Lykhach, H. Over, J. Libuda, V. Vonk and A. Stierle, A Combined Rotating Disk Electrode–Surface x-Ray Diffraction Setup for Surface Structure Characterization in Electrocatalysis, *Rev. Sci. Instrum*, 2022, **93**(6), 065111, DOI: **10.1063/5.0087864**.

19 J. Evertsson, F. Bertram, L. Rullik, G. Harlow and E. Lundgren, Anodization of Al(100), Al(111) and Al Alloy 6063 Studied in Situ with X-Ray Reflectivity and Electrochemical Impedance Spectroscopy, *J. Electroanal. Chem.*, 2017, **799**, 556–562, DOI: **10.1016/j.jelechem.2017.07.010**.

20 G. S. Harlow, S. Pfaff, G. Abbondanza, Z. Hegedüs, U. Lienert and E. Lundgren, HAT: A High-Energy Surface X-Ray Diffraction Analysis Toolkit, *J. Appl. Crystallogr.*, 2023, **56**(1), 312–321, DOI: **10.1107/S1600576723000092**.

